Polymer Chemistry

Akylidenefluorene-Isoindigo Copolymers with an Optimized Molecular Conformation for Spacer Manipulation, π- π Stacking and Its Application in Efficient Photovoltaic Devices

SCHOLARONE™
Manuscripts

Polymer Chemistry

RSC Publishing

ARTICLE

Akylidenefluorene-Isoindigo Copolymers with an Optimized Molecular Conformation for Spacer Manipulation, π- π Stacking and Its Application in Efficient Photovoltaic Devices

Min-Hee Choi,[a] Kwan Wook Song [a] and Doo Kyung Moon* [a]

D-(π)$_n$-A-type copolymers with different thienyl spacers(n= 0~2) between akylidenefluorene and isoindigo (P1, P2, P3) were synthesized via a Suzuki coupling reaction. As the spacer increased from a polymer (P1) without a spacer, the UV-Vis absorption maximum (λ_{max}) red- shifted, and the band gap decreased from 1.83 to 1.64 eV. The highest occupied molecular orbital (HOMO) levels of the polymers were increased by increasing the number of spacers. In addition, the facile intermixing due to better accessibility with the PCBM led to an increase in the hole mobility and J_{SC}. In contrast to P1 and P2, when the orientation of the P3 thin films was blended with PC$_{70}$BM in an X-ray diffraction (XRD) measurement, an increased face-on structure of the crystallinity was observed. The power conversion efficiency (PCE) of P3 showed 3.0% and reached 4.2% when it was fabricated an inverted device at 1:2 ratio with PC$_{70}$BM.

1. Introduction

Polymer solar cells (PSCs) have received considerable attention in academic research and industrial application in recent years due to their inexpensive manufacturing. In particular, the bulk heterojunction (BHJ) system, which employs a conjugated polymer (as the electron donor) and a fullerene (as the electron acceptor) blend, has been widely studied. For PSCs, enhanced molecular engineering technology of π-conjugated polymers has recently emerged as a major research area. To enhance the power conversion efficiency (PCE) of the PSCs, the opto-electronic properties of the π-conjugated polymer, which is a photoactive material, should be tuned. An ideal conjugated polymer for PSCs should satisfy the following conditions: low bandgap to enlarge the absorption region in the visible and near-infrared regions; high absorption coefficient; high hole mobility; a suitable highest occupied molecular orbital (HOMO)-lowest unoccupied molecular orbital (LUMO) level; and excellent miscibility with fullerene[1, 2]. The PCE of the PSCs was enhanced to more than 7~9% by identifying the relationship between the chemical structure of the polymer and its photovoltaic performance[3-6]. To verify the state-of-the-art device performance of the polymer, research focused on controlling the crystallinity of the polymer in the solid-state at the nanoscale is required[7-9].

Alberto Salleo et al. reported that increased solid-state packing via strong π-π stacking leads to a high crystallinity[10]. In addition, I. McCulloch et al. proposed polyalkylidenefluorene for application in solution-processable organic semiconductors, which have a high charge carrier mobility and environmental stability. Alkylidenefluorene is an electron-rich unit that has a rigid planar structure, and this unit increases the π- π stacking

of the resulting polymer, imparts high mobility, decreases the HOMO level, and facilitates efficient conjugation from the chain length direction[11]. The alkylidenefluorene homopolymer has a significantly small intermolecular distance (<0.4 nm) that facilitates a coplanar conformation [12].

In previous study, we reported that the energy level and steric hindrance of the polymer could be adjusted according to the location of the side chain in the D-π-A type polymer[8]. The results indicated that the polymer without side chains from the spacer and acceptor exhibited the lowest band gap due to aggregation caused by a strong π-stack and possessed a low solubility and molecular weight. However, when the side chain was implemented in the spacer, the lowest PCE was observed due to the steric hindrance and edge-on rich structure. Most semiconducting organic materials exhibit anisotropic charge transport properties, where the electric charges effectively move from a π-stacking direction[13, 14].

In the D-A-type polymer, Mikkel Jørgensen et al. adjusted the length of the spacer of the polymer with alkoxyphenyl-benzothiadiazole[15]. David G. Lidzey et al. published research results based on adjusting the length of the spacer of the anthracene-benzothiadiazole polymer. As the number of spacers increased, the band gap decreased, and the differences in Jsc and PCE were insignificant. UV-vis absorption spectra were red-shifted when the numbers of spacers were increased. Recently, Tajima et al. reported the dithienopyrrole-benzothiadiazole copolymers with some different opto-electric results when the spacer introduced. Their polymers showed blue-shift spectra[16].

In contrast, the solubility and energy levels of isoindigo, which allows for implementation of various side chains with two -N through lactam rings, can be easily tuned. Furthermore,

isoindigo has been successfully introduced in the field of organic electronics to form donor-acceptor (D-A) small molecules and polymers via a strong electron-deficient unit[17-20]. Isoindigo were consisted of planar moieties that can form strong π-π stacks in the solid state. The hole and electron mobilities of isoindigo-based D-A conjugated polymers are 0.81 and 0.66 $cm^2V^{-1}s^{-1}$, respectively[21]. However, the results of an X-ray crystal analysis of isoindigo confirmed that the disadvantageous generation a steric interaction in which a twist occurs near the central C=C bond between two indolinones[22]. Although the implementation of one thiophene between D-A units is known to enhance properties, limited studies have reported the implementation of bithiophene, which has primarily resulted in insoluble polymers.

In this study, alkylidenefluorene-isoindigo copolymers were synthesized using Suzuki coupling reaction and these copolymers exhibit good solubility even when several thiophenes were employed. Thiophene and bithiophene were applied as a π-bridge between the isoindigo and alkylidenefluorene donor moiety. The structure-property relationship was observed for the length of the spacer. The results confirmed that the increased spacers decreased the twist angle between the donor and acceptor, which lead to an enhancement in the planarity, crystallinity, and PCBM intercalation. By applying the polymer with the bithiophene spacers, as an active layer, Jsc and FF increased and PCE = 4.2%.

2. Results and Discussion

2.1 Polymer Synthesis
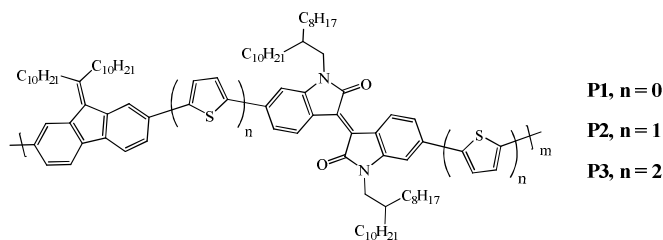
Figure 1. Isoindigo based conjugated polymers with alkylidenefluorene donating units.

Scheme 1 shows typical synthetic routes of the monomers and polymers, as shown in Figure 1. 9-(1'-decylundecylidene)fluorene (D1) was used as a donor and 6,6'-dibromo-N, N'-(2-octyldodecyl)isoindigo (A0), which is a well-known as organic dyes, was used as an acceptor. In addition, thiophene and bithiophene were applied as a conjugated linker for the indigo derivatives in A0 to synthesize A1 and A2, respectively, as shown in Scheme 1. Poly[2,7-bis-9-(1-decylundecylidene)fluorene-alt-N,N'-(2-octyl dodecyl)-6, 6'-π-isoindigo] (P1, P2, P3) were synthesized using a Suzuki coupling reaction with D1 and indigo derivatives (A0~A2) (Figure 1). The polymerization was performed at 90 °C for 48 h with Pd(PPh₃)₄(0), a 2M aqueous potassium carbonate solution, Aliquat 336 as a surfactant, and toluene : THF or DMF = 1 : 1 as a solvent. After the polymerization was completed, end-capping was performed using bromobenzene and phenyl boronic acid. The obtained powders were collected after being re-precipitated in methanol. Purification was performed sequentially with methanol, acetone, and chloroform using a Soxhlet apparatus. Finally, the

chloroform-soluble portion was re-precipitated in methanol. The obtained powders were reddish black (P1), blue-black (P2), and greenish black (P3) solids, and their yields were 76, 67, and 27%, respectively.

P1 and P2 were soluble in tetrahydrofuran (THF), chlorobenzene, and o-dichlorobenzene, and P3 was soluble only at an elevated temperature. The structure of the synthesized polymer determined using ¹H-NMR spectroscopy (see figure S1 in ESI). Isoindigo and the monomer of isoindigo with thiophene and bithiophene spacers were successfully synthesized, which was confirmed by the ¹H-NMR spectra. For the structure of the obtained polymers, the peak corresponding to P2 was determined to be between 7.08 and 6.8 ppm and 6.7~6.5 ppm due to the hydrogens combining with the 3, 4-carbon of the aromatic thiophene spacer. The peak corresponding to P3 was observed between 7.08 and 6.8 ppm and 6.7~6.5 ppm, which is the same peak observed for the of P2, due to the hydrogens combining with the 3, 4-carbon of the bithiophene spacer, and two additional hydrogens were found compared with the number of measured hydrogens in P2. In addition, the NMR spectra exhibited a decreased resolution and increasingly broadened peaks in the order of P1 to P3. This phenomenon is typically generated in polymers that have several carbon types, due to overlapping of all of the chemical shift anisotropy lines, which leads to a broad spectrum.

Table 1. Physical and thermal properties of polymers.

Polymer	Yield [%]	Mn[a] [kDa]	Mw[a] [kDa]	PDI[a]	Degree of polymerization[a]
P1	76	21.4	53.5	2.50	16
P2	67	28.2	75.0	2.66	19
P3	27	19.3	69.5	3.80	12

[a]Determined by GPC in tetrahydrofuran (THF) using polystyrene standards.

Table 1 lists the results of the measurements of molecular weights of the polymers. As shown in Table 1, P1, P2, and P3 have average molecular weights (Mn) of 21.4, 28.2, and 19.3 kDa, respectively, and broad PDI of 2.50, 2.66, and 3.80, respectively. In comparison to P1 and P3, P2 exhibited a high degree of polymerization due to the application of an appropriate thiophene linker. The planarity of P1, which does not have the spacer, decreased due to a large tilted angle between the donor and phenyl rings of the acceptor resulting in increased steric hindrance, which leads to a low degree of polymerization. Z. Peng et al. reported that when the distance of the phenyl and phenyl groups is close to the backbone of the polymers, the steric hindrance between the two groups increases, which makes it difficult to achieve a higher molecular weight[23]. Therefore, studies focused on effectively increasing the conjugation of the polymer main chain by improving the planarity between the donor and acceptor through the application of the spacer (e.g., P2 and P3) has been conducted. Jizheng Wang and David G. Lidzey et al. confirmed that the enhanced planarity between the donor and acceptor through the implementation of a spacer leads to a broad absorption range for the polymers and an excellent photovoltaic performance through the increased hole mobility[24, 25]. However, for P3, the small side-chain moieties within the repeating unit after the implementation of a double thiophene linker reduced the solubility of the polymers, which resulted in precipitation during the polymerization, leading to a low degree of polymerization.
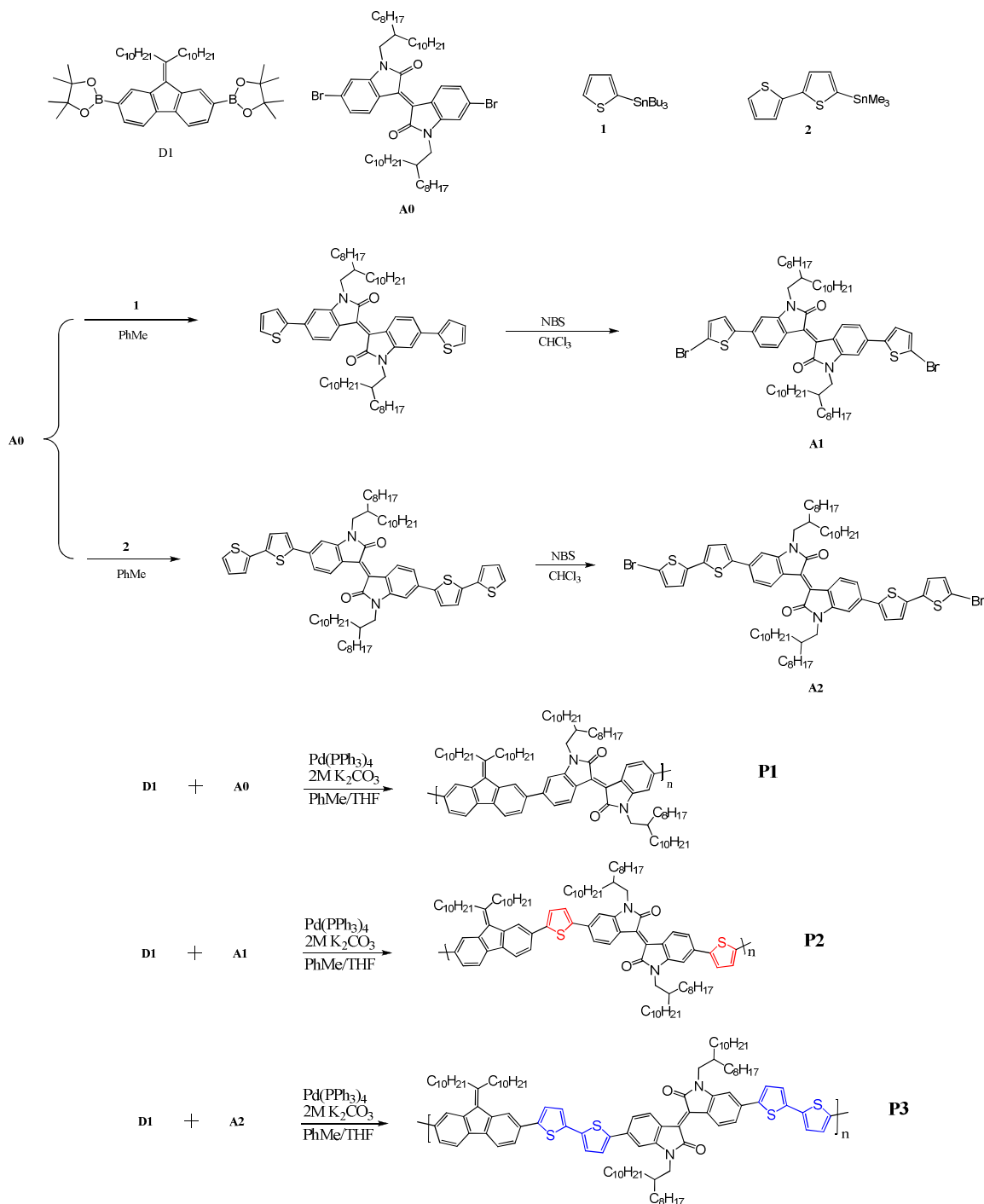
Scheme 1. Synthetic route to polymer

3.2 Optical and Electrochemical Properties

Figure 2 shows the UV-visible spectra for the solution and film phases of the three polymers. All of the polymers were measured after being dissolved in chloroform at a concentration of 10μg/ml. These results are summarized in Table 2. The maximum absorption peak (λ_{max}) of P1 was 321 mm in solution, and absorption coefficient at this time was calculated to be 3.0×10^4 $M^{-1}\cdot cm^{-1}$. In the film, the peak (λ_{max} = 330 nm) was red-shifted by 9 mm compared to that in solution. This red shift indicates that P1 has a strong π-stack tendency due to aggregation of the polymer in the solid state. The absorption edge of P1 was 678 nm, and the optical band gap

calculated according to this edge was 1.83 eV, which is the largest value of the synthesized polymers in this study. Therefore, when the spacer is absent from the main chain, the polymer has the largest bandgap as well as a correspondingly narrow absorption area. The maximum absorption peak (λ_{max}) of P2 was 615 nm in solution, and its absorption coefficient was calculated to be 4.0×10^4 $M^{-1}\cdot cm^{-1}$. In the film phase, the peak (λ_{max} = 604 nm) was blue-shifted by 11 nm compared to that in solution. The absorption edge of P2 was 725 nm, and the optical band gap that was calculated according to this edge was 1.71 eV. In addition, in comparison to P1, the absorption spectra of P2 were red-shifted by 60 nm in solution and by 35 nm in the film.
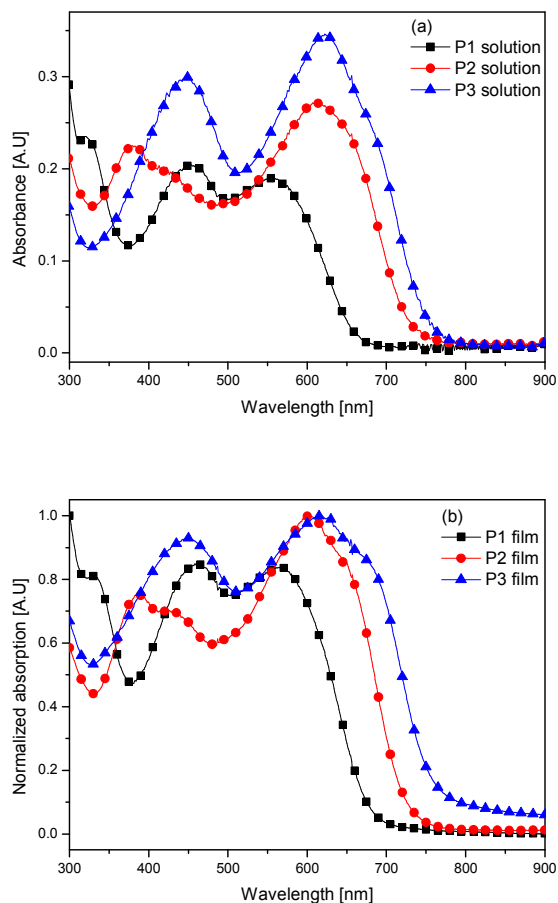
Figure 2. UV-Vis absorption spectra of polymers in solution (a) and film (b).

This confirms that P2 has a broader absorption area and a reduced band gap compared to P1 because the thiophene spacer was implemented between the alkylidenefluorene donor unit and isoindigo acceptor unit. This desrease in the band gap is due to the effective increase in the conjugation length of the polymers[26]. The UV-visible spectra of P3 are similar to those of P2. A maximum absorption peak (λ_{max}) of P3 was determined at 622 nm in solution, and its absorption coefficient was calculated to be 5.7×10^4 M$^{-1}\cdot$cm^{-1}. This value is greater than those for the P1 and P2 polymers, indicating that P3 facilitates a greater optical absorption. The peak (λ_{max} = 617 nm) of P3 in the film phase was blue-shifted by 5 nm compared to that in solution. The absorption edge of P3 was 756 nm, and the optical band gap that was calculated according to this edge was 1.64 eV. This band gap value is the lowest among those for the synthesized polymers in this study.

These results are consistent with the research results reported by David G. Lidzey[25]. By comparing the spectra of P2 and P3, the optical absorption of P3 was red-shifted in the long-wavelength region in both the solution and film. Because a longer π spacer was applied using bithiophene, the main chain of the polymer forms a more planar conformation and has an extended electronic delocalization leading to an increased conjugation length. The typical UV-visible spectra of the DA-type polymer primarily exhibit two absorption peaks. The peak in the high-energy area (300–500 nm) is caused by the π–π* transition of the donor segments (alkylidenefluorene derivatives) [27] and the peak in the low-energy

area (500–800 nm) is caused by the intramolecular charge transfer (ICT) transition (isoindigo units) between the donor and acceptor.[28]. The optical absorption graphs for P2 and P3 exhibited the form mentioned above, and the optical graph for P1 exhibited two optical absorption peaks in the range of 300–500 nm. Therefore, P1 exhibited a total of three peaks. The second absorption peak for P1, which was observed at 453 nm in solution and at 463 nm in the film, is generated by the n-π* transition due to aggregation of the expanded conjugation system through the C-N-C bonds of the alkylidenefluorene unit [29]. For P2 and P3, the effects of the expanded conjugation due to the spacer are greater than those due to the aggregation of the donor unit. Therefore, the n-π* transition is not observed due to a strong π–π* transition band. Because the UV spectrum of P1 was red-shifted when the phase changed from the solution to the film, the interaction between the polymer chains was enhanced due to the aggregation in the solid state. However, the UV spectrum of P2 and P3 tended to be blue-shifted when the phase changed from solution to film, indicating that the 2D π stacking between the polymer chains decreases. Therefore, the implemented spacer increases the electron-donating characteristics, which enhances the effects from the delocalized π-π* transition[30].

To confirm the effects of the thiophene spacer on the difference in the energy level, cyclic voltammograms of thin films for P1 ~ P3 were measured with 0.1 M tetrabutylammonium-hexafluorophosphate (TBAHFP) in an acetonitrile solution. The measurement results are shown in Figure 3 and summarized in Table 2. The oxidation onset potentials (E^{ox}_{onset}) of P1, P2, and P3 were +1.52, +1.35, and +1.23 V, respectively, and their calculated HOMO levels were -5.89, -5.72, and -5.60 eV, respectively. Because the air oxidation threshold was -5.27 eV, the HOMO level should be less than this value to ensure the oxidation stability of the materials[31].
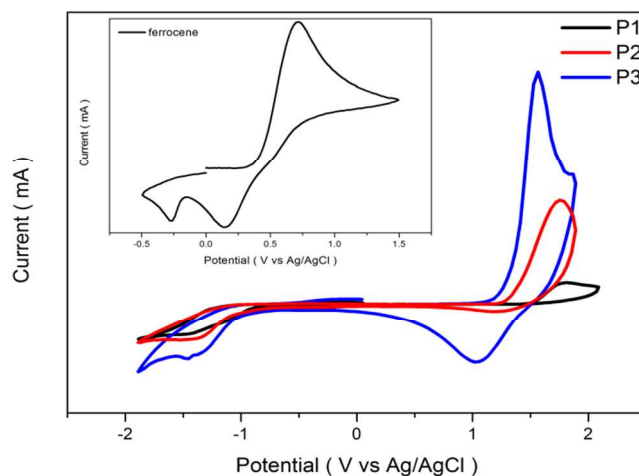
Figure 3. Cyclic voltamograms of Polymers

By increasing the amount of thiophene implemented in the spacer, the HOMO energy level of the polymers tended to increase from 5.89 to -5.60 eV because the increased thiophene spacers led to an increase in the electron-donating properties. These results are consistent with those reported by Yu's group that the HOMO level of the polymers in the push-pull system are primarily determined by the donor strength[32] and those reported by Lidzey et al. that the HOMO level increased due to the electron-donating properties of the thiophene spacer[25, 33]. In our previous study, the photovoltaic properties were investigated by synthesizing a D-π-A polymer series, such as poly[alkylidenefluorene-alt-di-2-thienyl-2,1,3-benzothiadiazole] [8]. The results of this study indicated that when the octoxy side chain was applied in benzothiadiazole, which served as

Table 2. Optical and electrochemical data of polymers.

Polymer	UV-vis absorption					$Eg^{op, a}$ [eV]	Cyclic voltammetry			
	CHCl3 solution		Film				E^{ox}_{onset} [V]	E^{red}_{onset} [V]	HOMO[b] [eV]	LUMO[c] [eV]
	λ_{max} [nm]	λ_{sh} [nm]	λ_{max} [nm]	λ_{sh} [nm]	λ_{onset} [nm]					
P1	321	453, 555	330	463, 569	678	1.83	1.52	-0.38	-5.89	-4.37
P2	615	376	604	389	725	1.71	1.35	-0.37	-5.72	-4.01
P3	622	447	617	447	756	1.64	1.23	-0.36	-5.60	-3.96

[a] Calculated from the intersection of the tangent on the low energetic edge of the absorption spectrum with the baseline

[b] $E_{HOMO \ (or \ LUMO)}$ = -[E_{onset}(vs Ag/AgCl) – $E_{1/2}$(Fc/Fc+ vs Ag/AgCl)] – 4.8eV

[c] LUMO = HOMO + E_g

an acceptor, the difference in the HOMO level of the polymers was insignificant. In addition, when an alkyl side chain was employed in the spacer, the HOMO level tended to be deep, and the difference in the HOMO level was between 0.04 and 0.15 eV. However, in this paper, the HOMO level of the polymers increased by +0.29 eV due to an increase in the spacer, which confirmed that the HOMO level of the polymers was affected more by the number of spacers (strength of donating properties of main chains of polymers) than by side-chain effects.

The LUMO levels calculated based on the differences in the HOMO energy levels and optical band gap energies of P1, P2, and P3 were -4.37 eV, -4.01 and -3.96 eV, respectively. The LUMO energy levels of the P2 and P3 polymers are within a reasonable range because the LUMO energy levels are far greater than those of PC$_{70}$BM (approximately - 4.3 eV). But, P1 showed deeper LUMO energy levels compared to PCBM and an energy difference ΔE of between the LUMO of the donor and the LUMO of the acceptor was only 0.07 eV. It suggests that the J_{SC} of PSC with P1:PC$_{70}$BM should be poor charge generation.

3.3 Computational Study of Polymers

Simulations using a density functional theory (DFT) were conducted to identify the electrical properties, molecular geometries, and electron density of the state distribution of the synthesized polymers. The DFT calculations were performed using Gaussian 09 with the hybrid B3LYP correlation functional and split valence 6-31G(d) basis set. Oligomers with two repeating units were selected for the calculation. The calculated HOMO and LUMO orbitals are shown in Figure 4.
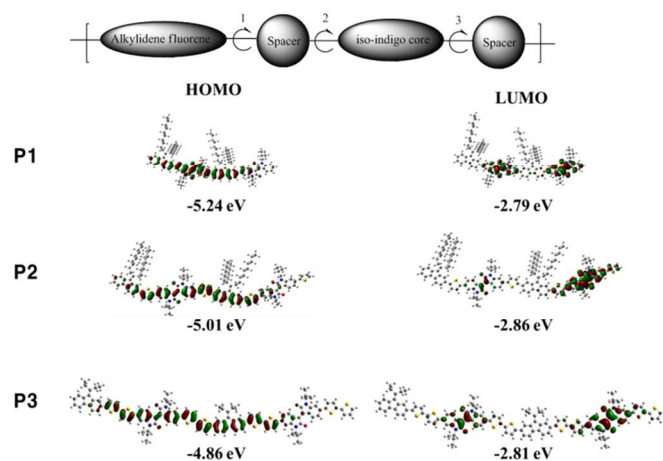
Figure 4. Calculated LUMO and HOMO orbitals for the dimer models of the polymers.

The HOMO orbitals are delocalized in the polymer main chain, and the LUMO orbitals were localized on the acceptor indigo dye

due to the structural characteristics of the quinoid formed between the non-bonding electron pairs of nitrogen and sulfur, which exhibit electron-withdrawing characteristics [34]. As measured by a cyclic voltammogram, the lowest HOMO level (-5.24 eV) was obtained for P1, and the highest HOMO level (-4.86 eV) was obtained for P3 due

to an increase in the electron-donating properties of the thiophene spacer.

The dihedral angles between the two spacer groups and the central isoindigo core and alkylidenefluorene were measured according to Figure 4, and the results are summarized in Table 3. Based on these results, the internal steric hindrance of the polymers was observed according to the different lengths of the spacers. Dihedral angle 1 of P1 was 35.5° and dihedral angle 1 of P2 and P3 were 24.2° and 25.9°, respectively, which decreased by 10° or more compared to when the spacer did not present. Therefore, the steric hindrance of P1 was significantly greater than that of the other two polymers. In addition, dihedral angles 2 and 3 of P2 were 23.4° and 23.9°, respectively, and dihedral angles 2 and 3 of P3 were 20.8° and 19.6°, respectively. As the length of the spacer increased, the tilting angle of the polymers decreased because P3, which has a longer bithiophene spacer than P2, provides broader spaces in which the side chains can be released in the alkylidenefluorene and isoindigo core to ensure solubility of the polymers. The steric hindrance effectively decreases the π-π stacking between the polymers and the charge transport [35].

Therefore, the implementation of a π linker reduces the steric hindrance between the alkylidenefluorene and the isoindigo core, the tilt angles decrease more as longer spacers are applied. Increased tilt angles break the conjugation reducing the current density during device manufacturing. Therefore, the current density of P3 will be the highest during the manufacture of OPV cells.

Table 3. Calculated parameters.

Polymer	dihedral angle (deg)			HOMO[cal.] [eV]	LUMO[cal.] [eV]
	1	2	3		
P1	35.5	-	-	-5.24	-2.79
P2	24.2	23.4	23.9	-5.01	-2.86
P3	25.9	20.8	19.6	-4.86	-2.81

3.4 XRD measurement

To better understand the ordering characteristics of thin films and the π linker effect of the polymer, X-ray diffraction measurements were conducted at annealing temperatures. X-ray diffraction measurements of the polymer films, measured in the out-of-plane mode, were used to analyse the ordering structure in Figure 5(a).
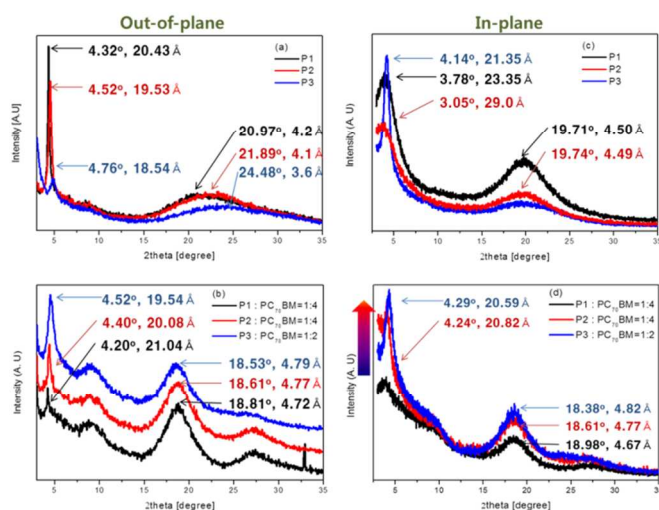
Figure 5. X-ray diffraction pattern of polymers on a silicon wafer and Polymer:PC$_{70}$BM blend on silicon wafer Out-of-plane mode (a), (b) and In-plane mode (c), (d).

The thin film of P1 and P2 measured in the out-of-plane mode exhibited clear, sharp diffraction peaks at 4.32° and 4.52°, which indicates the formation of a (100) lamellar structure with high crystallinity. The results of a calculation using Bragg's law ($\lambda = 2d\sin\theta$) indicated that the highly ordered (100) lamellar d-spacings (d_l) were 20.43 and 19.53 Å. However, unlike the other two polymers, P3 exhibited a small (100) peak at 4.76°, and the d_l calculated for this state was 18.54 Å. This is in good agreement with Erjun Zhou and Keisuke Tajima's work. Erjun Zhou et al. reported that dithienopyrrole-based donor–acceptor type copolymers with various thienyl spacers. In the out-of-plane XRD measurement, the polymer which doesn't have spacer showed diffraction peak near 6°. But, increasing the number of spacers, the polymers didn't show (100) diffraction peaks[16]. The broad diffraction peaks of the (010) crystal plans, which are related to the π-π stacking, were observed at 20.97°, 21.89°, and 24.48° for P1, P2, and P3, respectively. The π-π stacking distances (d_π) of P1, P2, and P3 were 4.2, 4.1, and 3.6 Å, respectively. The d_l- and d_π-spacing (i.e., the distances between the polymer chains of the P1–P3 polymers) decreased when going from P1 to P3. This result is in agreement with the DFT results where the tilt angle decreased as the spacer became longer, alleviating the steric hindrance between the alkylidenefluorene and the isoindigo core.

XRD measurements were conducted to validate the structural arrangement of the PCBM and polymer blended films (Figure 5(b)). Strong (010) diffraction peaks due to the crystallinity of fullerene were measured at 18.81°, 18.61°, and 18.53° in the out-of-plane measurements of the polymer : PC$_{70}$BM blend films. The interlamellar spacings of the P1~P3 : PC$_{70}$BM thin films calculated using the 2θ value of the (010) peaks were 4.72, 4.77, and 4.79 Å, respectively. These values increases by 052, 0.67, and 1.12 Å, respectively compared with the d_π value measured in the polymer thin film. This result means that PC$_{70}$BM has penetrated tightly between the polymer chains [36]. However, PC$_{70}$BM did not penetrate the intermolecular structure of P1 and P2, and they exist separately. In addition, the intensity of the (100) peak decreased for the diffraction peak of the P1 and P2 polymer thin films, confirming that blending with PC$_{70}$BM interrupted the molecular arrangement of P1 and P2. However, a higher order of the lamellar scattering was observed in the P3:PC$_{70}$BM blend film, because the intensity of the (100) peak, which was recorded to be very low when only the P3

polymer was measured, increased when PC$_{70}$BM was added.

Figure 3 (c) and (d) presents the XRD profiles of the polymer and polymer : PCBM blended thin films measured in the in-plane mode, respectively. The XRD profiles for P3 in the in-plane mode had one diffraction peak at low (2θ = 4.14°) angles, which suggests that the P3 thin films formed face-on structure. In contrast, the thin film of P1 and P2 showed XRD peaks at both low and high angles in the in-plane mode, demonstrating that this crystal structure had a mixed bimodal orientation. In figure 3(d), all of polymer : PCBM blend films showed XRD peaks at both low and high angles in the in-plane mode. The P3: PCBM blended thin film had the strongest diffraction peak at 4.29° in the in-plane mode. But, low angle diffraction peaks tended to decrease in the in-plane mode XRD profile during decreasing number of spacers. It means predominant crystalline structure within polymer:PC$_{70}$BM blend films was changed from edge-on to face-on when increased the number of spacers.

3.5 Photovoltaic Properties

To determine the photovoltaic (PV) properties as a function of the spacer, BHJ PSCs were fabricated. Figure 6(a) shows the J-V curves of the BHJ PCSs, and Figure 6(b) shows the incident photon to charge carrier efficiency (IPCE). The PV properties of the three polymers were evaluated by manufacturing PSC devices with ITO/PEDOT:PSS/polymer:PC$_{70}$BM/BaF$_2$/Ba/Al structures. All of the fabricated devices were encapsulated in a glove box. The J–V characteristics were measured under ambient atmosphere with an active area of 4mm^2, and their performances were measured under 100 mW/cm^2 AM 1.5G illumination. The ratio of polymer to PC$_{70}$BM was adjusted from 1:1 to 1:4 (by weight) and the optimized condition was 1:4(P1, P2) and 1:2(P3). The polymer active layers were spin-coated from solutions in σ -dichlorobenzene(ODCB). Table 4 and Table S2 summarize the photovoltaic response data including V$_{OC}$, J$_{SC}$, FF, and PCEs. OPV current density−voltage (J−V) plots, under standard illumination, for the solar cells based on P1~P3:PC$_{70}$BM active blends are shown in Figure 6.

In P1, the open circuit voltage (Voc) was 1.0 V, the short-circuit current density (Jsc) was 0.07 mAcm^2, and the FF was 49.1% to yield a PCE of 0.04 %. In P2, a PCE of 0.66% was observed under a Voc of 0.858 V, Jsc of 1.4 mA/cm^2, and FF of 54.2%, and P3 exhibited a PCE of 3.0% under a Voc of 0.798 V, Jsc of 7.3 mA/cm^2, and FF of 51.6%. Because the exciton dissociation rate was low due to the low extinction coefficient, wide band gap, and excessive steric hindrance, low Jsc values were recorded resulting in a low PCE for P1. When the spacer was used, the band gap decreased, and the extinction coefficient increased due to increase in conjugation length and planarity, which caused an increase in Jsc and device performance values. When PC$_{70}$BM was blended with P1–P3, the regularity of the molecular arrangement of P1 and P2 decreased while P3 formed a higher-order lamellar structure [37]. This result is in good agreement with the increase in crystallinity where the active layer of P3:PC$_{70}$BM exhibits a face-on rich structure, as shown in the XRD measurement in Figure 5. However, the Voc decrease. The Voc values of the devices created by the polymer:PC$_{70}$BM (i.e., blending the P2 and P3 polymers) were recorded to be 0.858 and 0.798 V, respectively. The V$_{OC}$ is determined according to the difference between the HOMO energy level in the polymers and the LUMO energy levels in PCBM. P1 exhibited the highest V$_{OC}$ because it has a deeper-lying HOMO level. The electron-donating characteristics were reinforced in P2 and P3 with the implementation of the spacers, leading to increases in the HOMO level with a reduction in the V$_{OC}$ values.

These devices exhibited adequately wide EQE graphs in the visible region (300–700 nm) and large EQE values in the absorbance
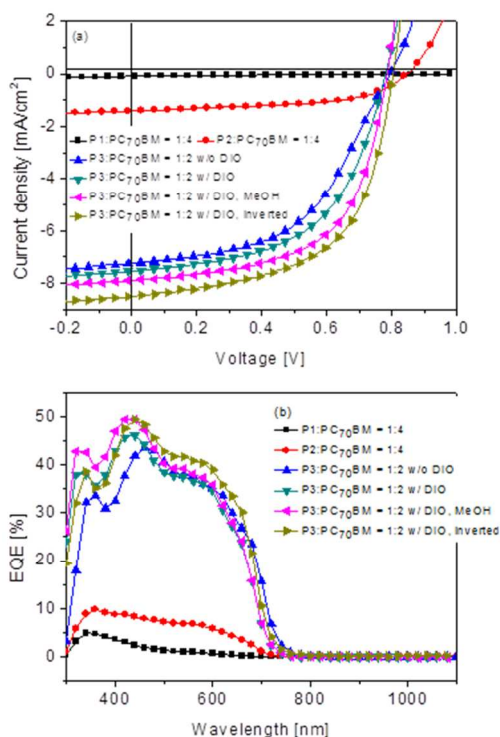
Figure 6. J–V curves of the PSC based on Polymer:PC$_{70}$BM (a) under the illumination of AM 1.5G, 100 mW/cm^2. The IPCE spectra of the PSC based on Polymer : PC$_{70}$BM (b).

range of 300~750 nm but lower values above 750 nm.

The P3:PC$_{70}$BM blend-based devices exhibited the highest EQE (up to 43.5%) at 460 nm, which agrees with the result for the highest photo current value. P1 and P2 recorded 4.85% and 9.77%, respectively.

Therefore, changes in the energy level of the polymers and steric hindrance are dependent on the implementation of a spacer and its length.

P3, which has the highest HOMO level due to bithiophene, exhibited the lowest Voc. But the small steric hindrance contributed to the Jsc greatly increasing by the approach of the PCBM and the

resulting increase in the crystallinity.

To optimize and enhance the performance of P3 device, 3 vol% 1,8-diiodooctane(DIO) was add as solvent additive. It leads to a significant 10% enhancement in PCE with a simultaneous improvement in Jsc (7.3 to 7.5 mA/cm^2) and FF (51.6 to 55.2%). Recently postdeposition methanol treatment has proven to be an effective method to obtain nanoscale morphology for active layer by controlling the phase separation between donor and acceptor. Methanol has been widely used in surface engineering by incorporation of interlayer in BHJ PSCs[38]. As shown in Figure 6 (a), after treating the active layer with methanol, the PCE is increased from 3.3 to 3.6% for the P3 device. It showed slightly increased a Jsc, from 7.5 to 7.7 mA/cm^2 and a FF from 55.2 to 57.6%. The PC$_{70}$BM molecules may migrate more easily between the polymer chains by methanol treatment, which then effectively increase the interfacial area between the polymers and the PC$_{70}$BM molecules with maintaining nanoscopically connected each domain. This is supported by results of the morphology studies (Figure 7).

Compared with conventional OPVs, inverted type devices can also take advantage of the vertical phase separation and concentration gradient in the active layer, which is naturally self-encapsulated because air-stable metals are used as the top electrode[39]. So we manufactured inverted PSC devices with ITO/ZnO/P3:PC$_{70}$BM/MoO$_3$/Ag structures, PCE is increased to 4.0%. It showed a Jsc = 8.2 mA/cm^2 and a FF = 58.7%.

3.6 Morphology analysis and charge carrier mobility

Hole mobility of the polymer is very important to the photovoltaic performance of BHJ solar cells. We used a space charge limited current (SCLC) model, which is based on the Poole–Frenkel law, to determine the hole mobility in blends containing the polymer and PC$_{70}$BM. The result can be obtained by plotting $\ln(JL^3/V^2)$ vs. $(V/L)^{1/2}$ and is shown in ESI*. Herein, J refers to the current density, d refers to the thickness of the device, and V = V$_{appl}$ −V$_{bi}$, where V$_{appl}$ is the applied potential and V$_{bi}$ is the built-in potential. Hole-only devices were fabricated with a diode configuration of ITO(170 nm)/PEDOT:PSS(40nm)/Polymer:PC$_{70}$BM/MoO$_3$(30nm)/Al(100nm).

According to Figures S2–S4 of $\ln(JL^3/V^2)$ vs. $(V/L)^{1/2}$ and the equation, the hole mobility of the three blended polymers are 5.76×10^{-5}, 4.61×10^{-4}, and 1.97×10^{-3} cm^{2}V^{-1}s^{-1}.

Table 4. Photovoltaic properties of polymers.

| polymer	device structure	Solvent + Additive	solvent treatment	PC$_{70}$BM ratios	Voc[V]	Jsc[mA/cm^2]	FF[%]	PCE[%]
P1	conventional	ODCB+none	none	1:4	1.0	0.07±0.003	49.1±1.4	0.04±0.006
P2	conventional	ODCB+none	none	1:4	0.858±0.02	1.4±0.2	54.2±1.4	0.66±0.04
P3	conventional	ODCB+none	none	1:2	0.798±0.02	7.3±0.3	51.6±0.9	3.00±0.1
P3	conventional	CB+DIO	none	1:2	0.778±0.02	7.5±0.2	55.2±2.0	3.3±0.1
	conventional	CB+DIO	MeOH		0.778±0.02	7.7±0.2	57.6±0.2	3.6±0.2
	inverted	CB+DIO	none		0.798	8.2±0.3	58.7±0.7	4.0±0.2

The P3:PCBM blend exhibited the highest mobility due to the high crystalline morphology of the blend film and the larger planar structure of the polymer.

The surface morphology of the polymer blend is another critical factor that determines the efficiency of PSCs. Therefore, the morphologies of the polymer:PCBM blend films were characterized using atomic force microscopy (AFM) and are shown in Figure S7.

The dark-colored and light-colored areas correspond to the PCBM domains and polymers, respectively. The surfaces of the P3:PC$_{70}$BM blended films were smooth with nanoscale features. The good intermixing between the polymer and PC$_{70}$BM resulted in the optimal formation of the channels in the polymers. This result agrees with the high Jsc in P3. However, the black dots due to the high aggregation of the PCBM domain was observed in the P1 and P2 blend films. A significant phase separation was observed, especially in P1, which had the roughest surface with a root-mean-square (RMS) roughness of 7 nm. This result is due to the difficulty PCBM experiences approaching the polymer chain due to significant steric hindrance. When a long π-linker was implemented in the polymer backbone for P1–P3, the RMS roughness tended to decrease, and J$_{SC}$ increased.

We also directly examined the surface morphology with and without methanol exposure via AFM. The AFM topography images are shown in Figure 7.
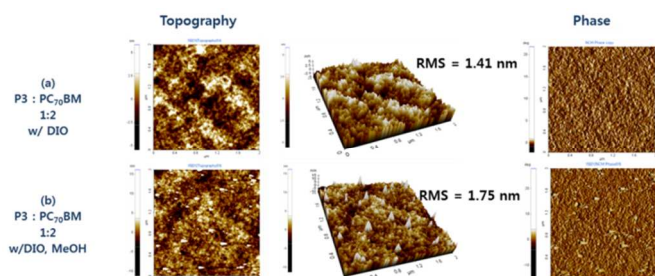
Figure 7. Topographic AFM images of Polymer:PC$_{70}$BM (a) P3: PC$_{70}$BM 1:2w/w with DIO ($2 \times 2\mu m^2$), (b) P3: PC$_{70}$BM 1:2w/w with DIO + MeOH treatment ($2 \times 2\mu m^2$)

In the case of P3:PC$_{70}$BM blends, it could be observed that the blend film without solvent exposure exhibited relatively course phase separation between the polymer and PC$_{70}$BM with a relatively large (100−500 nm) PC$_{70}$BM globular clusters that may originate during the drying of the film. In contrast, after solvent treatment, the surface of the blend film demonstrated a more uniform distribution of P3 and PC$_{70}$BM. And the formation of interpenetrating morphologies at the small scale of 100−200 nm PC$_{70}$BM clusters for the methanol-treated device. This relatively smooth surface and more fine structure are beneficial to the charge transportation, thus leading to an increase in Jsc, as well as the device efficiency.

3. Experimental

3.1 Materials
All starting materials were purchased from Sigma Aldrich and Alfar Aesar, and used without further purification. Toluene and tetrahydrofuran (THF) were distilled from benzophenone ketyl and sodium. The following compounds were synthesized following modified literature procedures : 2,7-Bis(4,4,5,5-tetramethyl-1,3,2-dioxaborolan-2-yl)-9-(1-decylundecylidene)fluorene (AF)[27, 40], 6,6'-dibromo-N, N'-(2-octyldodecyl)isoindigo (A0)[41], 2T[42].

3.2 Polymerizations

3.2.1 Poly[2,7-bis-9-(1-decylundecylidene)fluorene-alt-N, N'-(2-octyldodecyl)-6, 6'-isoindigo] (P1)
Reddish black solid, 0.285 g (yield = 76 %). ^{1}H NMR (400 MHz, CDCl$_3$, d) : 9.30-9.25 (m, 2H), 8.08 (s, 2H), 7.91-7.89 (m, 2H), 7.45 (m, 2H), 7.37-7.34 (m, 2H), 7.08 (m, 2H), 3.77 (m, 4H), 2.91 (m, 3H), 2.00-1.82 (d, 2H), 1.40-1.21 (m, 92H), 0.83 (s, 18H).

3.2.2 Poly[2,7-bis-9-(1-decylundecylidene)fluorene-alt-N, N'-(2-octyldodecyl)-6, 6'-dithiphen-2-yl-isoindigo] (P2)
Blue black solid, 0.29 g (yield = 67 %). ^{1}H NMR (400 MHz, CDCl$_3$, d) : 9.15-8.95 (m, 2H), 8.10-6.80 (m, 12H), 6.70-6.50 (m, 2H), 3.80-3.60 (m, 4H), 2.95-2.65 (m, 4H), 2.00-0.95 (m, 98H), 0.95-0.65 (s, 16H).

3.2.3 Poly[2,7-bis-9-(1-decylundecylidene)fluorene-alt-N, N'-(2-octyldodecyl)-6, 6'-di-2,2'-bithiphen-5-yl-isoindigo] (P3)
Greenish black solid 0.14 g (yield = 27 %). ^{1}H NMR (400 MHz, CDCl$_3$, d) : 9.15-8.95 (m, 2H), 8.10-6.80 (m, 14H), 6.70-6.50 (m, 2H), 3.80-3.60 (m, 4H), 2.95-2.65 (m, 3H), 2.00-0.95 (m, 98H), 0.95-0.65 (s, 16H).

3.3 Measurements
The ^{1}H-NMR (400 MHz) spectra were recorded using a Brüker AMX400 spectrometer in CDCl$_3$, and the chemical shifts were recorded in units of ppm with TMS as the internal standard. The absorption spectra were recorded using an Agilent 8453 UV-visible spectroscopy system. The solutions that were used for the UV-visible spectroscopy measurements were dissolved in chloroform at a concentration of 10 μg/ml. The films were drop-coated from the chloroform solution onto a quartz substrate. All of the GPC analyses were carried out using THF as the eluent and a polystyrene standard as the reference. The TGA measurements were performed using a TG 209 F3 thermogravimetric analyzer. The cyclic voltammetric waves were produced using a Zahner IM6eX electrochemical workstation with a 0.1 M acetonitrile (substituted with nitrogen for 20 min) solution containing tetrabutylammonium hexafluorophosphate (Bu$_4$NPF$_6$) as the electrolyte at a constant scan rate of 50 mV/s. ITO, a Pt wire, and silver/silver chloride [Ag in 0.1 M KCl] were used as the working, counter, and reference electrodes, respectively. The electrochemical potential was calibrated against Fc/Fc+. The HOMO levels of the polymers were determined using the oxidation onset value. Onset potentials are values obtained from the intersection of the two tangents drawn at the rising current and the baseline changing current of the CV curves. The LUMO levels were calculated from the differences between the HOMO energy levels and the optical band-gaps, which were determined using the UV-vis absorption onset values in the films. The current density–voltage (J–V) curves of the photovoltaic devices were measured using a computer-controlled Keithley 2400 source measurement unit (SMU) that was equipped with a Class A Oriel solar simulator under an illumination of AM 1.5G (100 mW/cm^2). Topographic images of the active layers were obtained through atomic force microscopy (AFM) in tapping mode under ambient conditions using an XE-100 instrument.

3.4 Photovoltaic cell fabrication and treatment
All the bulk-heterojunction PV cells were prepared using the following device fabrication procedure. The glass/indium tin oxide (ITO) substrates [Sanyo, Japan(10 Ω/γ)] were sequentially patterned lithographically, cleaned with detergent, ultrasonicated in deionized water, acetone, and isopropyl alcohol, dried on a hot plate at 120 ˚C for 10 min, and treated with oxygen plasma for 10 min to improve the contact angle just before film coating. Poly(3,4-ethylene-

dioxythiophene):poly(styrene-sulfonate) (PEDOT:PSS, Baytron P 4083 Bayer AG) was passed through a 0.45-mm filter before being deposited on ITO at a thickness of ca. 32 nm by spin-coating at 4000 rpm in air, and then dried at 120 °C for 20 min inside a glove box. A blend of 1-(3-methoxycarbonyl)propyl-1-phenyl-[6,6]-C71 (PC71BM) and the polymer [1:2 (w/w), 1:4 (w/w)] at a concentration of 7.5 mgmL^{-1} in chlorobenzene was stirred overnight, filtered through a 0.2-mm poly(tetrafluoroethylene) (PTFE) filter, and then spin-coated (500–3000 rpm, 30 s) on top of the PEDOT:PSS layer. The device was completed by depositing thin layers of BaF$_2$ (1 nm) and Ba (2 nm) as an electron injection cathode, followed by the deposition of a 200-nm-thick aluminum layer at pressures less than 10^{-6} torr. The active area of the device was 4 mm^2. Finally, the cell was encapsulated using UV-curing glue (Nagase, Japan).

The hole-only devices were fabricated with a diode configuration of ITO(170nm)/PEDOT:PSS(40nm)/PQCQT:PC$_{70}$BM(50nm)/MoO$_3$(30nm)/Al(100nm). The hole mobility of the active layers was calculated from the SCLC using the J–V curves of the hole-only devices in the dark as follows:

$$J = \frac{9}{8}\varepsilon_r\varepsilon_0\mu_{h(e)}\frac{V^2}{L^3}\exp\left(0.89\sqrt{\frac{V}{E_0 L}}\right)$$

where ε_0 is the permittivity of free space (8.85X10^{-14} F/cm); ε is the dielectric constant (assumed to be 3, which is a typical value for conjugated polymers) of the polymer; μ is the zero-field mobility of holes (electrons); L is the film thickness; and V = V$_{appl}$–V$_r$ + V$_{bi}$), where V$_{appl}$ is the applied voltage to the device, V$_r$ is the voltage drop due to series resistance across the electrodes, and V$_{bi}$ is the built-in voltage.

4. Conclusions

In this study, we successfully synthesized three polymers (i.e., P1, P2, and P3) that use alkylidene fluorene as donors and isoindigo derivatives as acceptors using the Suzuki coupling reaction by adjusting the thiophene spacer length. As the number of thiophene spacers increased, the band gap of polymers decreased and the HOMO level tended to increase. Although P1 and P2 exhibited an edge-on rich orientation in the XRD measurements, when the polymers were blended with PC$_{70}$BM, P1 and P2 only exhibited a peak due to the crystallinity of PC$_{70}$BM and a substantial decrease in the (100) peak of the polymer. P3 allowed for easier access of PC$_{70}$BM, an increase face-on crystallinity peak was observed in in-plane mode of XRD measurements. Although V$_{OC}$ decreased due to the increase in the HOMO level resulting from the implementation of the bithiophene spacer, the best performance was observed when PCE = 4.2% in the P3:PC$_{70}$BM structure (1:2, w/w).

Acknowledgements

Notes and references

^{a} Department of Materials Chemistry and Engineering, Konkuk University, 1 Hwayang-dong, Gwangjin-gu, Seoul 143-701, Korea.
Tel.: +82-2-450-3498, Fax: +82-2-444-0765
E-mail: dkmoon@konkuk.ac.kr

1. K. W. Song, M. H. Choi, H. J. Song, S. W. Heo, J. Y. Lee and D. K. Moon, *Sol. Energy Mater. Sol. Cells*, 2014, **120, Part A**, 303-309.
2. M. H. Choi, K. W. Song, S. W. Heo, Y. W. Han and D. K. Moon, *J. Ind. Eng. Chem.*
3. Z. He, C. Zhong, X. Huang, W.-Y. Wong, H. Wu, L. Chen, S. Su and Y. Cao, *Adv. Mater.*, 2011, **23**, 4636-4643.
4. C. Cabanetos, A. El Labban, J. A. Bartelt, J. D. Douglas, W. R. Mateker, J. M. J. Fréchet, M. D. McGehee and P. M. Beaujuge, *J. Am. Chem. Soc.*, 2013, **135**, 4656-4659.
5. M. A. Green, K. Emery, Y. Hishikawa, W. Warta and E. D. Dunlop, *Progress in Photovoltaics: Research and Applications*, 2013, **21**, 1-11.
6. H. J. Song, D. H. Kim, E. J. Lee, J. R. Haw and D. K. Moon, *Sol. Energy Mater. Sol. Cells*, 2014, **123**, 112-121.
7. A. T. Yiu, P. M. Beaujuge, O. P. Lee, C. H. Woo, M. F. Toney and J. M. J. Fréchet, *J. Am. Chem. Soc.*, 2011, **134**, 2180-2185.
8. K. W. Song, H. J. Song, T. H. Lee, S. W. Heo and D. K. Moon, *Polymer Chemistry*, 2013, **4**, 3225-3235.
9. M. S. Chen, J. R. Niskala, D. A. Unruh, C. K. Chu, O. P. Lee and J. M. J. Fréchet, *Chem. Mater.*, 2013, **25**, 4088-4096.
10. A. Salleo, R. J. Kline, D. M. DeLongchamp and M. L. Chabinyc, *Adv. Mater.*, 2010, **22**, 3812-3838.
11. J. Liu, H. Choi, J. Y. Kim, C. Bailey, M. Durstock and L. Dai, *Adv. Mater.*, 2012, **24**, 538-542.
12. M. Heeney, C. Bailey, M. Giles, M. Shkunov, D. Sparrowe, S. Tierney, W. Zhang and I. McCulloch, *Macromolecules*, 2004, **37**, 5250-5256.
13. V. Coropceanu, J. Cornil, D. A. da Silva Filho, Y. Olivier, R. Silbey and J.-L. Brédas, *Chem. Rev.*, 2007, **107**, 926-952.
14. M. R. Hammond, R. J. Kline, A. A. Herzing, L. J. Richter, D. S. Germack, H.-W. Ro, C. L. Soles, D. A. Fischer, T. Xu, L. Yu, M. F. Toney and D. M. DeLongchamp, *ACS Nano*, 2011, **5**, 8248-8257.
15. J. Eggert Carlé, J. Wenzel Andreasen, M. Jørgensen and F. Christian Krebs, *Sol. Energy Mater. Sol. Cells*, 2010, **94**, 774-780.
16. Y. Geng, J. Cong, K. Tajima, Q. Zeng and E. Zhou, *Polymer Chemistry*, 2014, **5**, 6797-6803.
17. J. Mei, K. R. Graham, R. Stalder and J. R. Reynolds, *Org. Lett.*, 2010, **12**, 660-663.
18. R. Stalder, J. Mei and J. R. Reynolds, *Macromolecules*, 2010, **43**, 8348-8352.
19. X. Xu, P. Cai, Y. Lu, N. S. Choon, J. Chen, X. Hu and B. S. Ong, *Journal of Polymer Science Part A: Polymer Chemistry*, 2013, **51**, 424-434.
20. D. H. Kim, A. L. Ayzner, A. L. Appleton, K. Schmidt, J. Mei, M. F. Toney and Z. Bao, *Chem. Mater.*, 2012, **25**, 431-440.
21. T. Lei, J.-H. Dou, Z.-J. Ma, C.-J. Liu, J.-Y. Wang and J. Pei, *Chemical Science*, 2013, **4**, 2447-2452.
22. Y. K. Voronina, D. B. Krivolapov, A. V. Bogdanov, V. F. Mironov and I. A. Litvinov, *Journal of Structural Chemistry*, 2012, **53**, 413-416.
23. Z. Peng, W. Si, S. Lin, H. Miao, H. Fu, M. Xie, H. Ma, H. Zeng and Z. Su, *Eur. Polym. J.*, 2002, **38**, 1635-1643.
24. Z. G. Zhang and J. Wang, *Journal of Materials Chemistry*, 2012, **22**, 4178-4187.

25.   M. S. Almeataq, H. Yi, S. Al-Faifi, A. A. B. Alghamdi, A. Iraqi, N. W. Scarratt, T. Wang and D. G. Lidzey, *Chem. Commun.*, 2013, **49**, 2252-2254.

26.   C. L. Chochos and S. A. Choulis, *Prog. Polym. Sci.*, 2011, **36**, 1326-1414.

27.   M. Heeney, C. Bailey, M. Giles, M. Shkunov, D. Sparrowe, S. Tierney, W. Zhang and I. McCulloch, *Macromolecules*, 2004, **37**, 5250-5256.

28.   R. Stalder, J. Mei, J. Subbiah, C. Grand, L. A. Estrada, F. So and J. R. Reynolds, *Macromolecules*, 2011, **44**, 6303-6310.

29.   T. Yasuda, T. Imase and T. Yamamoto, *Macromolecules*, 2005, **38**, 7378-7385.

30.   L. Dong, Y.-C. Chiu, C.-C. Chueh, A.-D. Yu and W.-C. Chen, *Polymer Chemistry*, 2014.

31.   D. M. de Leeuw, M. M. J. Simenon, A. R. Brown and R. E. F. Einerhand, *Synth. Met.*, 1997, **87**, 53-59.

32.   H. Zhou, L. Yang and W. You, *Macromolecules*, 2012, **45**, 607-632.

33.   H. Yi, S. Al-Faifi, A. Iraqi, D. C. Watters, J. Kingsley and D. G. Lidzey, *J. Mater. Chem.*, 2011, **21**, 13649-13656.

34.   Z. Ma, E. Wang, M. E. Jarvid, P. Henriksson, O. Inganas, F. Zhang and M. R. Andersson, *J. Mater. Chem.*, 2012, **22**, 2306-2314.

35.   H. Zhou, L. Yang, S. Xiao, S. Liu and W. You, *Macromolecules*, 2010, **43**, 811-820.

36.   W. Lee, G.-H. Kim, S.-J. Ko, S. Yum, S. Hwang, S. Cho, Y.-H. Shin, J. Y. Kim and H. Y. Woo, *Macromolecules*, 2014, **47**, 1604-1612.

37.   N. C. Cates, R. Gysel, Z. Beiley, C. E. Miller, M. F. Toney, M. Heeney, I. McCulloch and M. D. McGehee, *Nano Letters*, 2009, **9**, 4153-4157.

38.   K. Kranthiraja, K. Gunasekar, W. Cho, M. Song, Y. G. Park, J. Y. Lee, Y. Shin, I.-N. Kang, A. Kim, H. Kim, B. Kim and S.-H. Jin, *Macromolecules*, 2014, **47**, 7060-7069.

39.   S. Kim, J. H. Koh, X. Yang, W. S. Chi, C. Park, J. W. Leem, B. Kim, S. Seo, Y. Kim, J. S. Yu, J. H. Kim and E. Kim, *Advanced Energy Materials*, 2014, **4**, n/a-n/a.

40.   J.-Y. Lee, W.-S. Shin, J.-R. Haw and D.-K. Moon, *Journal of Materials Chemistry*, 2009, **19**, 4938-4945.

41.   H. Bronstein, Z. Chen, R. S. Ashraf, W. Zhang, J. Du, J. R. Durrant, P. Shakya Tuladhar, K. Song, S. E. Watkins, Y. Geerts, M. M. Wienk, R. A. J. Janssen, T. Anthopoulos, H. Sirringhaus, M. Heeney and I. McCulloch, *J. Am. Chem. Soc.*, 2011, **133**, 3272-3275.

42.   K. Parab, K. Venkatasubbaiah and F. Jäkle, *Journal of the American Chemical Society*, 2006, **128**, 12879-12885.

TABLE CAPTIONS

Table 1. Physical and thermal properties of polymers.

Table 2. Optical and electrochemical data of polymers.

Table 3. Calculated parameters.

Table 4. Photovoltaic properties of polymers.

Table 1. Physical and thermal properties of polymers.

Polymer	Yield [%]	Mn^a [kDa]	Mw^a [kDa]	PDI^a	Degree of polymerization[b]
P1	76	21.4	53.5	2.50	16
P2	67	28.2	75.0	2.66	19
P3	27	19.3	69.5	3.80	12

[a]Determined by GPC in tetrahydrofuran (THF) using polystyrene standards.

Table 2. Optical and electrochemical data of polymers.

Polymer	UV-vis absorption					$Eg^{op, a}$ [eV]	Cyclic voltammetry			
	CHCl$_3$ solution		Film				E^{ox}_{onset} [V]	E^{red}_{onset} [V]	HOMO[b] [eV]	LUMO[c] [eV]
	λ_{max} [nm]	λ_{sh} [nm]	λ_{max} [nm]	λ_{sh} [nm]	λ_{onset} [nm]					
P1	321	453, 555	330	463, 569	678	1.83	1.52	-0.38	-5.89	-4.37
P2	615	376	604	389	725	1.71	1.35	-0.37	-5.72	-4.01
P3	622	447	617	447	756	1.64	1.23	-0.36	-5.60	-3.96

[a]Calculated from the intersection of the tangent on the low energetic edge of the absorption spectrum with the baseline

[b] $E_{HOMO \text{ (or LUMO)}} = -[E_{onset}(\text{vs Ag/AgCl}) - E_{1/2}(\text{Fc/Fc}^+ \text{ vs Ag/AgCl})] - 4.8\text{eV}$

[c] $LUMO = HOMO + E_g$

Table 3. Calculated parameters.

Polymer	dihedral angle (deg)			$HOMO^{cal.}$ [eV]	$LUMO^{cal.}$ [eV]
	1	2	3		
P1	35.5	-	-	-5.24	-2.79
P2	24.2	23.4	23.9	-5.01	-2.86
P3	25.9	20.8	19.6	-4.86	-2.81

Table 4. Photovoltaic properties of polymers.

polymer	device structure	Solvent + Additive	solvent treatment	$PC_{70}BM$ ratios	Voc[V]	Jsc[mA/cm2]	FF[%]	PCE[%]
P1	conventional	ODCB+none	none	1:4	1.0	0.07±0.003	49.1±1.4	0.04±0.006
P2	conventional	ODCB+none	none	1:4	0.858±0.02	1.4±0.2	54.2±1.4	0.66±0.04
P3	conventional	ODCB+none	none	1:2	0.798±0.02	7.3±0.3	51.6±0.9	3.00±0.1
	conventional	CB+DIO	none		0.778±0.02	7.5±0.2	55.2±2.0	3.3±0.1
P3	conventional	CB+DIO	MeOH	1:2	0.778±0.02	7.7±0.2	57.6±0.2	3.6±0.2
	inverted	CB+DIO	none		0.798	8.2±0.3	58.7±0.7	4.0±0.2

FIGURE CAPTIONS

Figure 1. Isoindigo based conjugated polymers with alkylidenefluorene donating units.

Figure 2.UV-Vis absorption spectra of polymers in solution (a) and film (b).
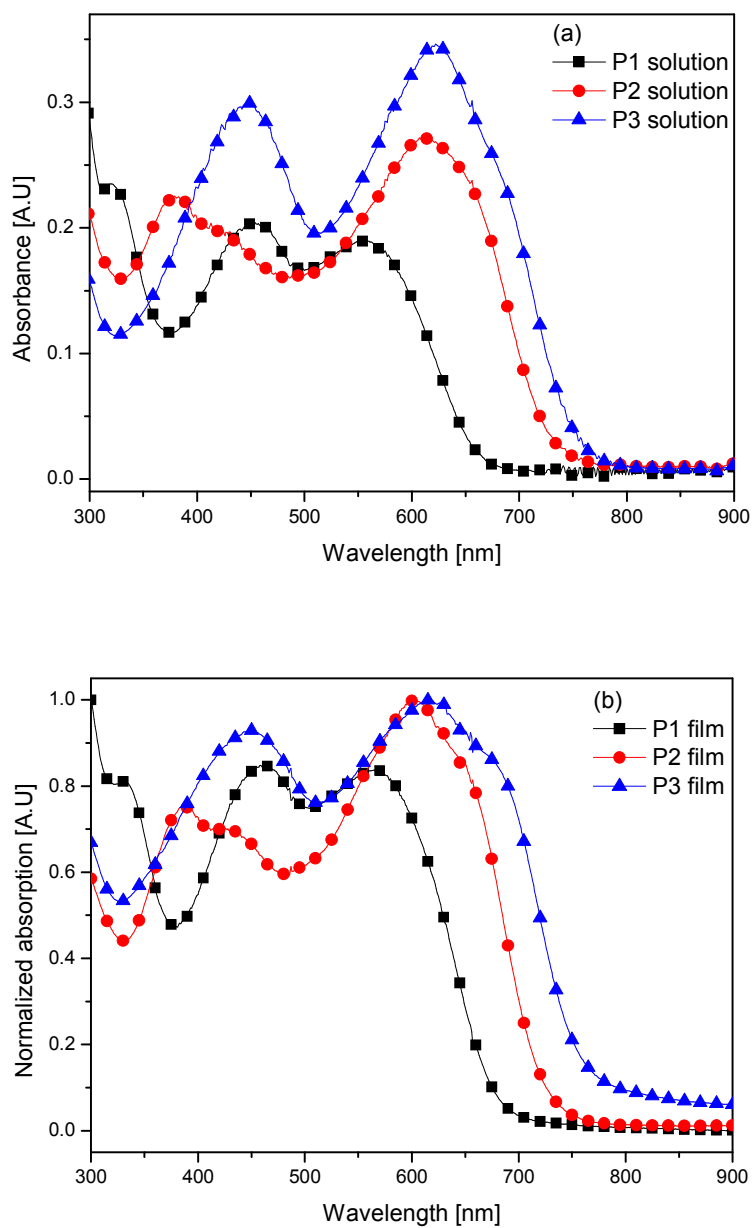
Figure 3. Cyclic voltamograms of Polymers
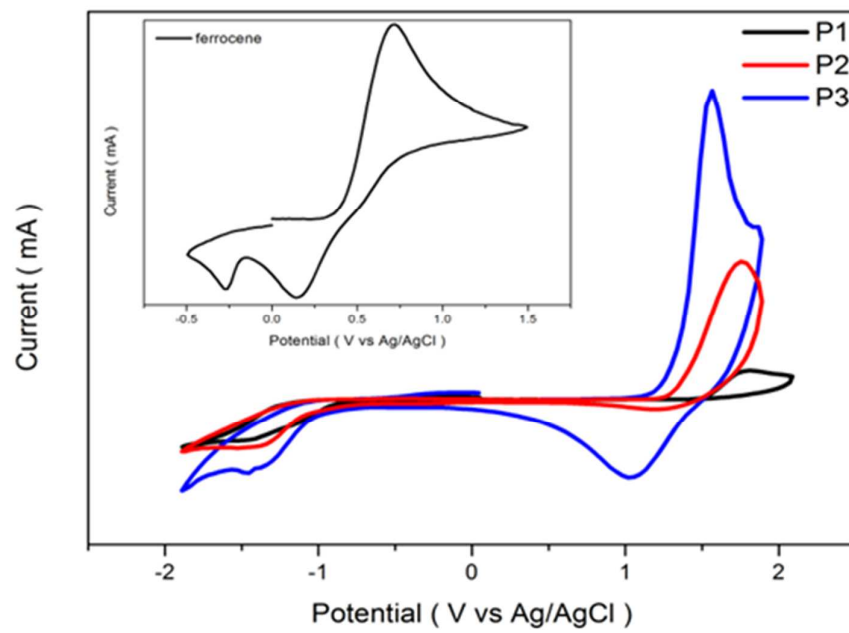
Figure 4. Calculated LUMO and HOMO orbitals for the monomer unit and the dimer models of the polymers.

Figure 5. X-ray diffraction pattern of polymers on a silicon wafer and Polymer:$PC_{70}BM$ blend on silicon wafer Out-of-plane mode (a), (b) and In-plane mode (c), (d).

Figure 6. J–V curves of the PSC based on Polymer:$PC_{70}BM$ (a) under the illumination of AM 1.5G, 100 mW/cm^2. The IPCE spectra of the PSC based on Polymer : $PC_{70}BM$ (b).

Figure 7. Topographic AFM images of Polymer:$PC_{70}BM$ (a) P3: $PC_{70}BM$ 1:2w/w with DIO ($2 \times 2\mu m^2$), (b) P3: $PC_{70}BM$ 1:2w/w with DIO + MeOH treatment ($2 \times 2\mu m^2$)

SCHEME TITLES

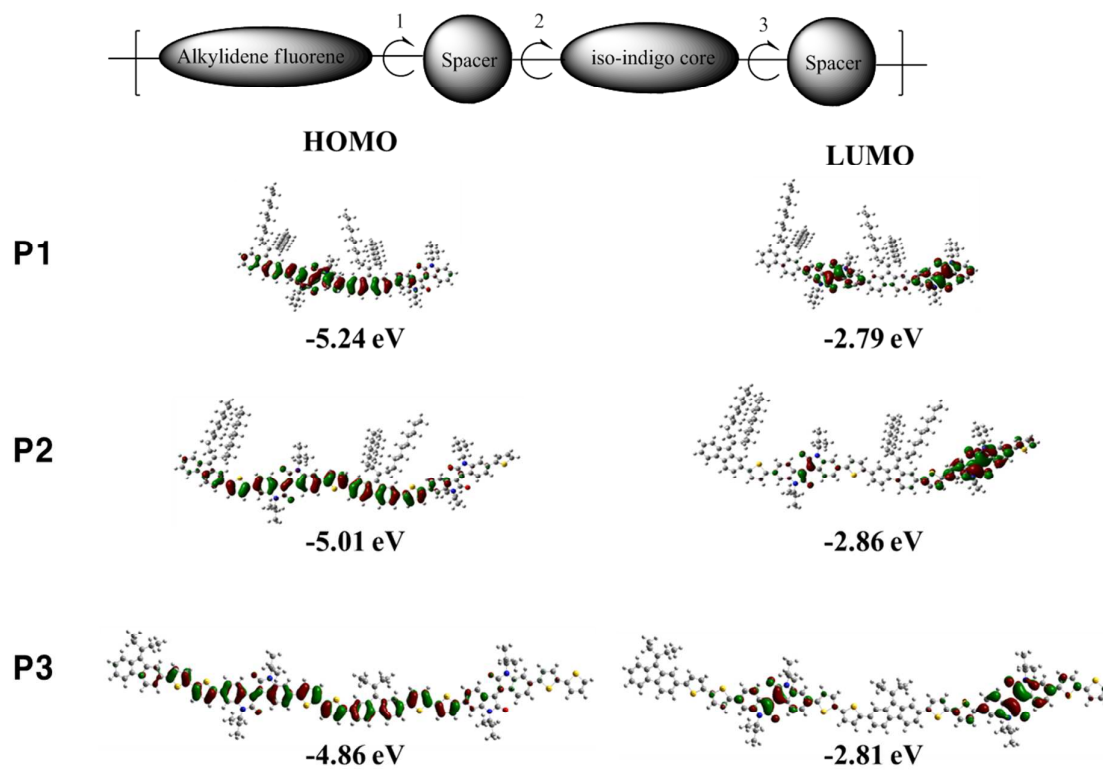**Scheme 1.** Synthetic route to polymers.

Figure 1. Isoindigo based conjugated polymers with alkylidenefluorene donating units.
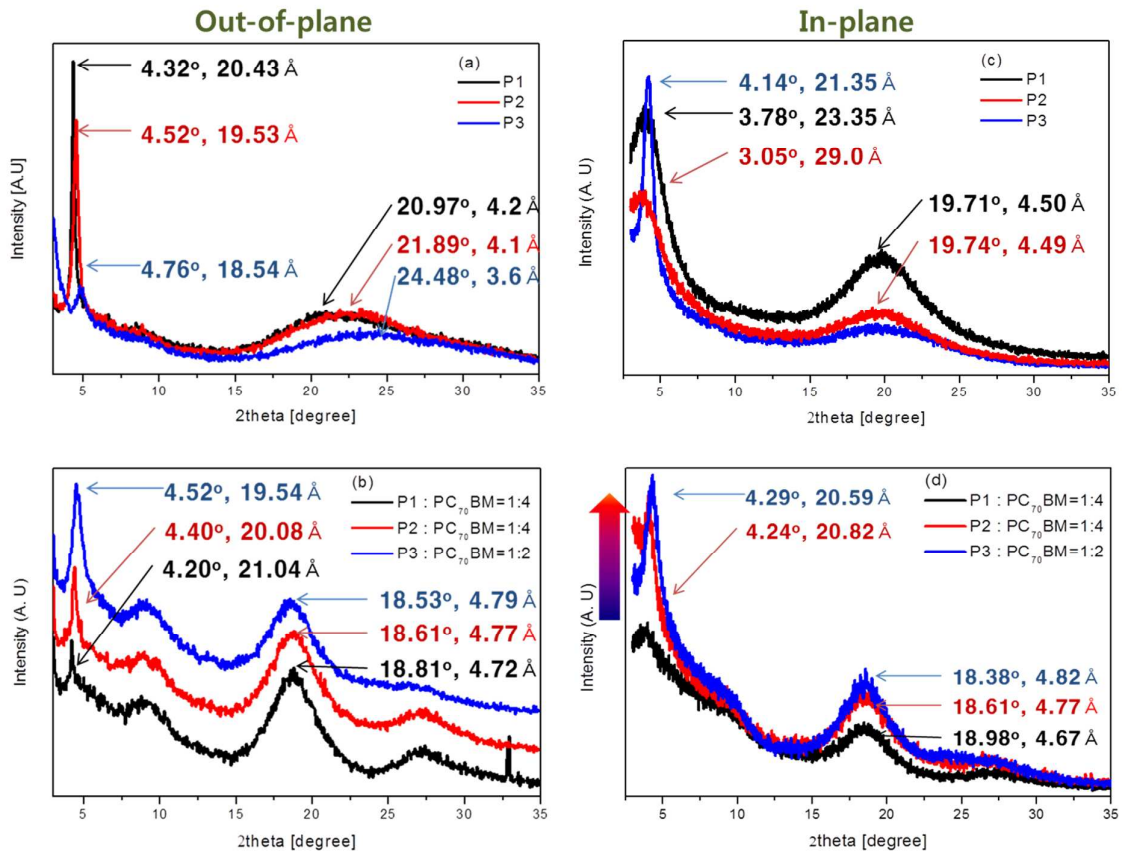

P1, n = 0

P2, n = 1

P3, n = 2

Figure 2.UV-Vis absorption spectra of polymers in solution (a) and film (b).
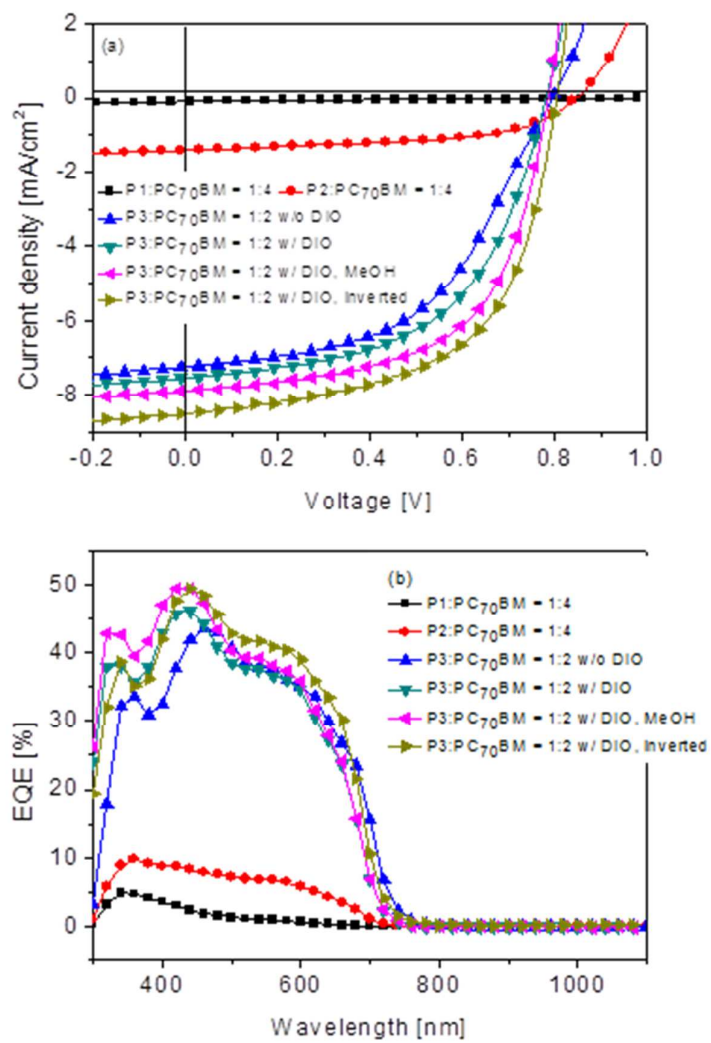
Figure 3. Cyclic voltamograms of Polymers

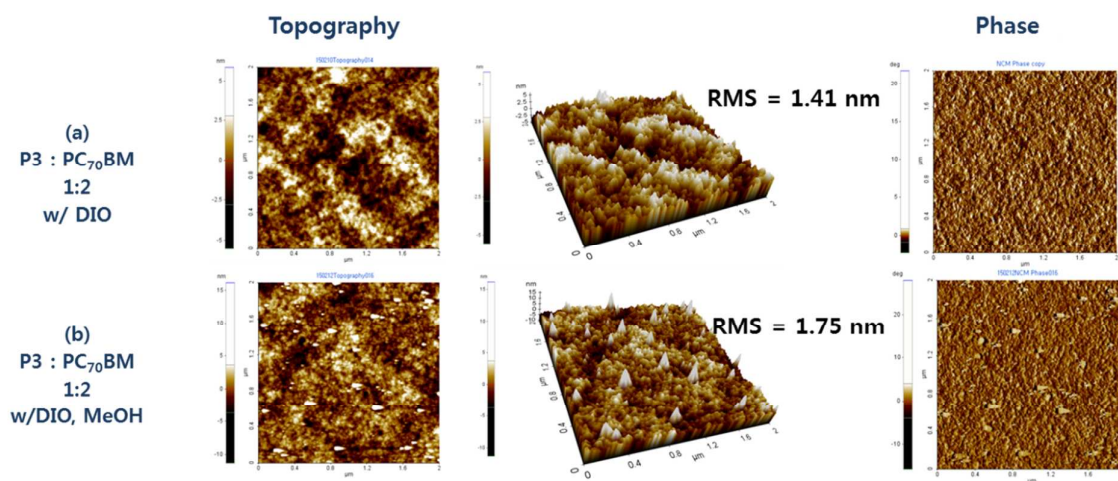**Figure 4.** Calculated LUMO and HOMO orbitals for the monomer unit and the dimer models of the polymers.

HOMO

LUMO

P1

-5.24 eV

-2.79 eV

P2

-5.01 eV

-2.86 eV

P3

-4.86 eV

-2.81 eV

Figure 5. X-ray diffraction pattern of polymers on a silicon wafer and Polymer:$PC_{70}BM$ blend on silicon wafer Out-of-plane mode (a), (b) and In-plane mode (c), (d).

Figure 6. J–V curves of the PSC based on Polymer:PC$_{70}$BM (a) under the illumination of AM 1.5G, 100 mW/cm^2. The IPCE spectra of the PSC based on Polymer : PC$_{70}$BM (b).

Figure 7. Topographic AFM images of Polymer:PC$_{70}$BM (a) P3: PC$_{70}$BM 1:2w/w with DIO

($2 \times 2\mu m^2$), (b) P3: PC$_{70}$BM 1:2w/w with DIO + MeOH treatment ($2 \times 2\mu m^2$)

Scheme 1. Synthetic route to polymers.